



## Fluoride removal from drinking water using alumina adsorbent: batch and column experiments and working efficiency of engineered pilot plant

Muhammad Anas<sup>a,b,\*</sup>, Tahir Rafique<sup>b</sup>, Faisal Soomro<sup>a</sup>, Syed Nawazish Ali<sup>a</sup>

<sup>a</sup>Department of Chemistry, University of Karachi, Karachi, Pakistan, Tel. +92-323-2391345; Fax: +92-21-34641847; email: muhammadanas\_raza@yahoo.com

<sup>b</sup>Applied Chemistry Research Centre, PCSIR Laboratories Complex, Karachi – 75280, Pakistan

Received 23 October 2019; Accepted 1 November 2020

---

### ABSTRACT

Groundwater of the Thar Desert in Sindh province of Pakistan is known to have high fluoride concentration whose use for drinking purpose has led to a catastrophic prevalence of dental and skeletal fluorosis. Therefore, as a remedial measure to this problem, with an aim to bring fluoride levels in drinking water below the WHO limit of 1.5 mg/L, adsorption experiments have been carried out in this study in the batch and column modes and extended to the pilot scale investigations using alumina as the adsorbent. The batch mode experiments helped optimize the adsorption parameters such as adsorption time, adsorbent dose, and pH and the values were found to be 50 min, 2.0 g, and 6–7, respectively. Batch adsorption data further showed greater compatibility with Freundlich adsorption isotherm as well as pseudo-second-order model. The thermodynamic experiments revealed that the process is endothermic and spontaneous with Gibb's free energy ranging from –7.56 to –8.13 kJ/mol. A percentage removal of almost 95% in the batch mode was encouraging to carry the study to the column mode which represents a more pragmatic approach. Column experiments were carried out in a column of 33 cm length and 3.4 cm of the internal diameter which resulted in the breakthrough adsorption capacity of 4.98 mg/g at an initial fluoride concentration of 10 mg/L. Thomas and Yoon–Nelson adsorption models fitted well with the data with high values of determination coefficients. The maximum adsorption capacity  $Q_m$  and the rate constant  $K_{TH}$  obtained via Thomas model were found to be 8.82 mg/g and 0.0012 L/min mg, respectively, and the values of  $K_{YN}$  and  $\tau$  from Yoon–Nelson model were found to be 0.0128 min<sup>-1</sup> and 426.83 min, respectively. The column containing 5.0 g of alumina reached exhaustion after passing 7.1 L of 10.3 mg/L fluoride solution. It was subsequently regenerated with 1% NaOH with a desorption efficiency of 92%. Based on these results, a pilot plant was designed that contained 60 kg bed of alumina in a vessel of 13 inch internal diameter and 60 inch height. Experiments with pilot plant revealed that the plant can serve around 20,000 L of fluoride-safe drinking water if the initial fluoride concentration of the water is approximately 10 mg/L. The plant was successfully used up to the third cycle with decreasing efficiency of fluoride removal. These results are highly encouraging and pragmatic which will be helpful in engineering a real-time plant for the people of Thar desert to provide them with a fluoride-safe drinking water and overcome the menace of the fluorosis completely from the area.

*Keywords:* Adsorption; Desorption; Pilot-scale; Thomson model; Yoon-Nelson model

---

\* Corresponding author.

## 1. Introduction

As per World Health Organization (WHO), beside arsenic and nitrate, fluoride is considered one of the greatest chemical concerns of water for human consumption [1]. Fluoride is variably present on different segments of earth including crustal rocks, soil, river water, groundwater, and sea water [2]. The contamination of groundwater by fluoride is due to its extensive distribution in the geological environment and slow dissolution of fluoride containing minerals in rocks [3,4]. Incidences of high fluoride in groundwater have been witnessed in number of areas around the world especially the developing countries [5,6]. In Lake Nakuru, Kenya the natural fluoride concentration has been reported as high as 2,800 mg/L [7].

Accumulation of fluoride in groundwater has been a threat all around the globe as groundwater is the predominant source of human intake of fluoride [8]. The maximum permissible limit of fluoride in groundwater, set by WHO is 1.5 mg/L [1]. An excess intake of fluoride has been linked with severe health related effects characterized by irreversible and permanent deformities of bones and teeth known as skeletal and dental fluorosis respectively [9]. At adequate fluoride levels in the range of 1.50–4.60 mg/L dental fluorosis is observed and at certain higher levels that exceeds 5 mg/L symptoms of skeletal fluorosis are visualized [10].

Hydrochemical studies have shown that groundwater resources of Thar Desert in Pakistan are also highly affected with fluoride and endemic fluorosis has been observed in whole region with different intensities, including dental and skeletal fluorosis irrespective of age and gender [11]. The granitic basement of Thar Desert is rich in fluoride bearing minerals and influence of different geochemical processes elevates the groundwater with fluoride. Since people of Thar Desert completely rely on this groundwater for drinking purpose therefore a substantial area of Desert is affected by fluoride toxicity and its impacts on human health are severe in the form of prevalence of fluorosis.

These circumstances emphasize the importance of defluoridation studies which has prompted the development of numerous defluoridation techniques including adsorption, reverse osmosis, coagulation and precipitation, and electrodialysis [12]. Among these techniques, adsorption is unique due to its wide range of application and cost-effectiveness. An extensive list of materials has been compiled by Bhatnagar et al. [13] showing variety of adsorbents for defluoridation which includes, among others, alumina and aluminum-based adsorbents, iron-based sorbents, mixed metal oxides, carbon based sorbent, and natural materials. Among those adsorbents, activated alumina has been classified as the best demonstrated available technology (BDAT) by the WHO and USEPA due to its greater affinity and selectivity for fluoride [14]. Therefore, number of reports have presented the insight into the fluoride adsorption onto alumina and alumina-based adsorbents [15–19].

As far as the methodology of adsorption studies is concerned, batch mode is predominantly reported which is usually limited to the treatment of small volumes of effluent and is useful in determining the effectiveness of the adsorbent in terms of adsorption capacity and other thermodynamic and kinetic parameters. The batch mode has found

numerous uses in industry, however, from a drinking water perspective where bulk volumes are treated, adsorption with column have found more acceptance because the functionality of the column mode of adsorption is closer to the real-time plants. The adsorption of fluoride using alumina as an adsorbent in a column mode has been previously studied [20–22]. The experiments of the present study are part of an extensive study to propose a practical solution in the form of a defluoridation plant workable in the Thar desert to provide the inhabitants of the Thar desert with the fluoride-free drinking water. The novelty of the present study lies in the experiments related to the defluoridation pilot plant which will give a realistic estimate of the parameters required for the real plants to be installed in the coming future.

## 2. Materials and methodology

Commercial alumina, 28 × 48 Tyler mesh dimensions was purchased from BASF India with the pore volume 0.52 cc/g, surface area 380 m<sup>2</sup>/g, and bulk density of 40 lb/ft<sup>3</sup>. All the reagents and chemicals used in this study were of AR grade and were purchased from local markets of Karachi.

### 2.1. Analytical method

Stock solution of 1,000 mg/L fluoride was prepared in 1 L volumetric flask by dissolving 2.21 g of anhydrous sodium fluoride in deionized water (conductivity < 1 μS/cm). All the standard solutions were prepared by appropriate dilution of the stock solution with deionized water. The pH of deionized water was about 6.5–7.0, and all the experiments were conducted at ambient temperature (30°C ± 2°C). The fluoride concentration in the influent and effluent were determined by using a fluoride ion-selective electrode coupled with Thermo Scientific Orion 5-Star pH/ISE/DO/conductivity meter. Total ionic strength adjustment buffer (TISAB-IV) was prepared by dissolving 58 g of sodium chloride, 57 mL of glacial acetic acid, and 150 mL of 6 M NaOH solution with a little deionized water, and the volume was made up to 1,000 mL. Samples for fluoride analyses were diluted to 1:1 with TISAB-IV solution to maintain the pH of solution at 5.5 and to eliminate the interference of complexing ions. The fluoride ion-selective electrode was calibrated prior to each experiment to determine the slope and intercept of the electrode.

### 2.2. Batch mode studies

The batch experiments were conducted to study the effect of variables like contact time, adsorbent dosage, initial solution pH, and initial fluoride concentration and temperature on the defluoridation. Equilibrium time was optimized by taking 0.5 g alumina with 10 mg/L initial fluoride solution, shaken for the different interval of time from 10 to 100 min. Concentration variable was optimized from 10 to 30 mg/L initial concentration at constant dose of adsorbent. Effect of pH on defluoridation by alumina was studied between pH 2.0 and 12.0. For temperature variation, a batch of fixed volume of varying fluoride concentration (i.e., 10–30 mg/L) with optimized amount of alumina and time was run in a temperature controlled incubated shaker

(JEIO TECH, Korea, model number IST-3075R) at temperature ranging from 25°C to 40°C.

The percent adsorption capacity was calculated from the following equations:

$$\% \text{Adsorption} = \left( \frac{C_i - C_f}{C_i} \right) 100 \quad (1)$$

$$\% Q_e = \frac{(C_i - C_f)V}{m} \quad (2)$$

where  $Q_e$  is the mg of fluoride adsorbed per unit g of the adsorbent called adsorption capacity,  $m$  is the mass of adsorbent, and  $V$  is the volume of fluoride solution,  $C_i$  and  $C_f$  are the initial and final concentrations of fluoride, respectively.

### 2.3. Column studies

Break through curve was studied to examine the performance of adsorbent in dynamic mode and to evaluate its sorption capacity at break through point. For this purpose, fixed amount of alumina was introduced in column of known frit, 33 cm length and 3.4 cm diameter. Keeping WHO recommended limit of fluoride in drinking water as break through concentration, pre-determined concentration of fluoride solution was passed through the column at fixed flow rate. The contact between solid phase of adsorbent and fluoride in liquid phase of solution allowed an interaction which resulted in adsorption of fluoride. The point when fluoride concentration in fixed volume of the effluent was found to be equal or closer to 1.5 mg/L, was considered as break through point and mg of fluoride adsorbed on g of adsorbent was calculated as the sorption capacity at that point. Similarly, when the concentration of influent and effluent of column became closer or identical the column was considered exhausted and then regenerated.

Similar approach was adopted for desorption studies for the regeneration of column and concentration of NaOH was optimized for the maximum desorption. For this purpose, NaOH solutions of different strength were passed through the exhausted column and fluoride level in effluent was determined to estimate the desorption efficiency of a strength of NaOH for regeneration of exhausted column.

### 2.4. Pilot plant studies

To estimate the efficiency of pilot defluoridation plant, the breakthrough point study was extended to pilot plant scale. For this purpose, defluoridation bed of 60 kg with alumina was housed in a vessel of dimensions 13-inch internal diameter and 60-inch height. A batch of fluoride solution of 10 mg/L was passed through the fixed bed with high flow rates of up to 30 L per minute. The mean residual concentration of fluoride in the effluent was determined by taking the sample of effluent at initial, middle, and near the end of passage of single batch. The bed was regenerated after attaining the breakthrough point (i.e., at 1.5 mg/L) with 1% NaOH solution and then reused for the next cycle.

## 3. Results and discussion

### 3.1. Batch mode adsorption studies

#### 3.1.1. Equilibrium time

Fig. 1a reflects the impact of contact time on percent fluoride removal and it demonstrates that a removal efficiency of almost 84% has been achieved within 50 min of time after which it becomes constant suggesting that at the equilibrium has been established. At initial stage, adsorption was rapid due to the available vacant surface sites. After 50 min, the repulsive forces between the adsorbed  $F^-$  and the bulk phase  $F^-$  make it difficult for the remaining vacant surface sites to be occupied. Fig. 1b shows that adsorption capacity reaches a maximum of 0.745 mg/g during a time interval of 40–50 min and it remains almost constant afterward showing that equilibrium was established, and process approached monolayer formation.

#### 3.1.2. Adsorbent dose

The removal efficiency of alumina in terms of percentage removal at optimized time and different adsorbent doses is shown in Fig. 1c. The obtained data demonstrates that removal efficiency increased with an increase in adsorbent dose and nearly 94.44% of  $F^-$  was adsorbed at 2.0 g of alumina. However, after 2.0 g, there was no significant increment in  $F^-$  removal. Therefore, the 2.0 g adsorbent dose was used in further studies.

#### 3.1.3. Equilibrium concentration

The effect of initial fluoride concentration on removal efficiency of alumina in terms of percentage removal was investigated by running inlet concentration of fluoride solution in the range from 10 to 30 ppm. The results have been graphically presented in Fig. 1d which depicts a generally increasing pattern with 84%–90% removal. Since uptake of  $F^-$  from solution to the solid phase of adsorbent depends on fluoride to the available surface ratio of adsorbent, therefore, it may be concluded that adsorption efficiency increased due to increase in  $F^-$  to available surface ratio.

#### 3.1.4. Equilibrium pH

The effect of pH on the fluoride removal efficiency of alumina was studied in the pH range of 2–12 and results are shown in Fig. 2. The obtained data demonstrates that adsorption was maximum at the near neutral pH of 6–7 and quite low at both ends of this range of pH. In the acidic pH range, formation weak hydrofluoric acid along with chemical and electrostatic interaction of the oxide surface and fluoride ion plays important role in decreasing the adsorption efficiency of alumina. At higher pH (higher than neutral pH) the adsorption is lower because of stronger competition with hydroxide ions on adsorbent surface even though the oxide surface is positively charge [23].

#### 3.1.5. Adsorption isotherm modeling

Isotherm studies explain the feasibility of adsorption mechanism and defines the surface nature and affinity of

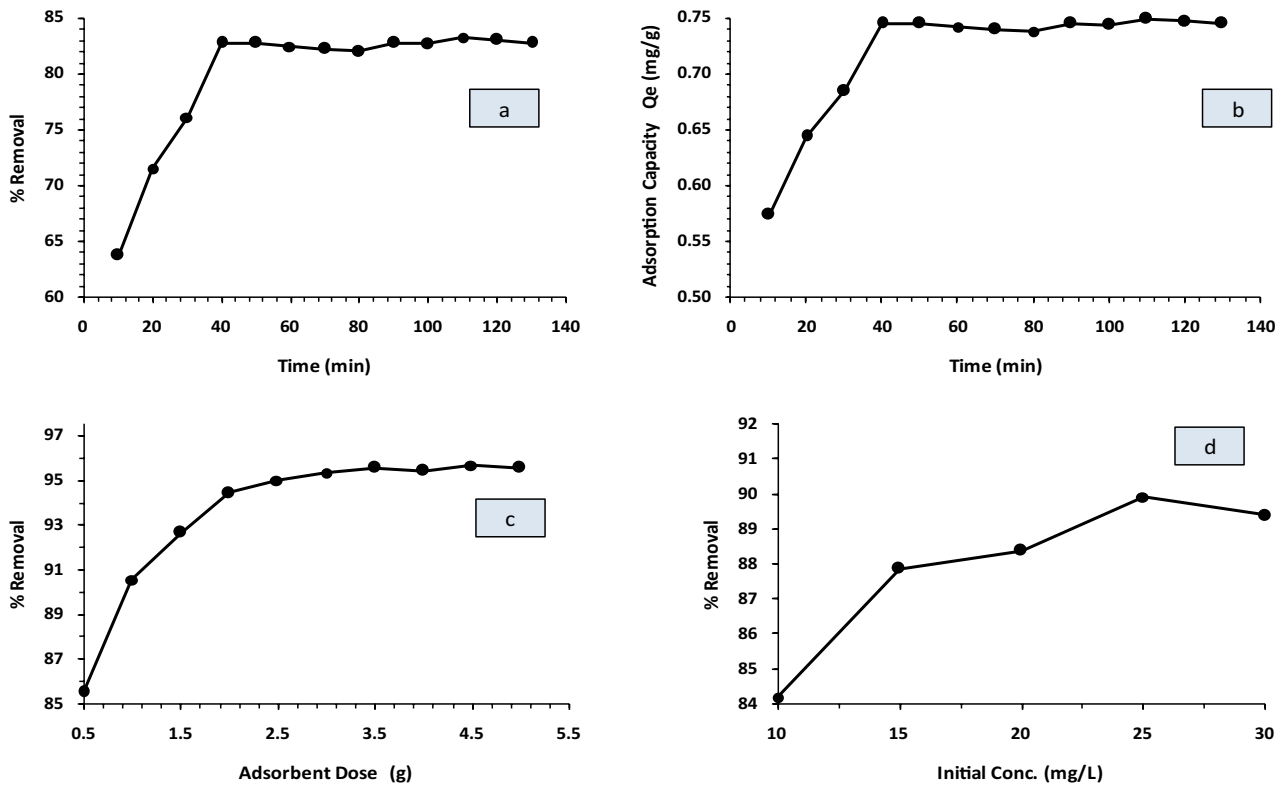


Fig. 1. (a–d) Optimization of batch adsorption parameters.

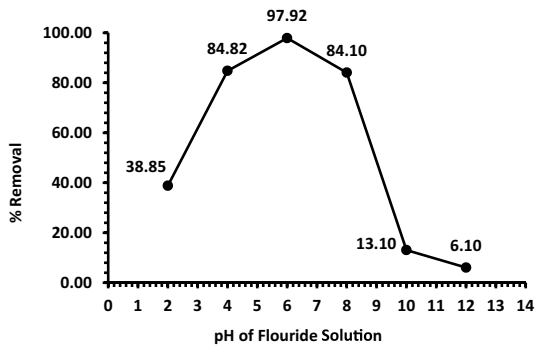


Fig. 2. Optimization of pH for the removal of fluoride using alumina.

the adsorbent. The obtained data was integrated with well-known Langmuir, Freundlich, and Dubinin–Radushkevich (D–R) isotherm models whose linear forms are given below:

Langmuir isotherm model linearized equation:

$$\frac{C_e}{Q_e} = \frac{1}{K_L Q_{\max}} + \frac{C_e}{Q_{\max}} \quad (3)$$

where  $C_e$  (mg/L) is the equilibrium concentration,  $Q_e$  (mg/g) is the sorption capacity,  $K_L$  is Langmuir constant,  $Q_{\max}$  (mg/g) is the monolayer capacity.

The constants  $K_L$  the feasibility of Langmuir isotherm can be determined by calculating the separation factor ( $R_L$ ) using following expression:

$$R_L = \frac{1}{(1 + K_L C_i)} \quad (4)$$

where  $K_L$  is the Langmuir constant and  $C_i$  (mg/L) is the initial concentration. Value  $R_L = 0$  indicates irreversible adsorption,  $R_L = 1$  linear, and  $R_L > 1$  unfavorable and  $R_L$  values between 0 to 1 favorable adsorption and  $Q_{\max}$  can be calculated from the slope and intercept of the plots of  $C_e/Q_e$  vs.  $C_e$ .

Freundlich adsorption model linearized equation:

$$\ln Q_e = \ln K_F + \frac{1}{n} \ln C_e \quad (5)$$

where  $n$  and  $K_F$  both are Freundlich constants their values can be derived from the slope and intercept respectively of the plots of  $\ln Q_e$  against  $\ln C_e$  (Figs. 3a and b). The slope of the plot is given by  $1/n$  and it shows adsorption intensity and surface heterogeneity whereby a value close to zero indicates more heterogeneity and chemisorption.

Dubinin–Radushkevich (D–R) isotherm linearized equation:

$$\ln Q_e = \ln q_D - \beta_D RT \ln \left( 1 + \frac{1}{C_e} \right)^2 \quad (6)$$

where  $\ln(1 + 1/C_e)^2$  is reduced into  $\epsilon^2$ ,  $q_D$  (mg/g) is the monolayer capacity of adsorbent,  $\beta_D$  is a constant related to adsorption energy,  $R$  (J/mol K) is a gas constant,  $T$  is absolute temperature,  $Q_e$  and  $C_e$  have usual meanings.

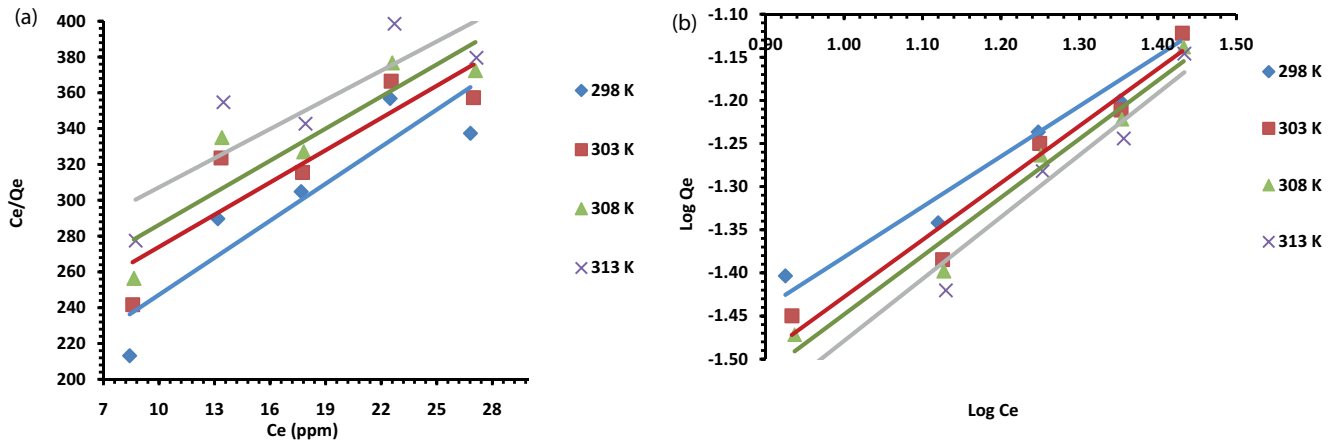


Fig. 3. Plots of (a) Langmuir and (b) Freundlich isotherm model for the removal of fluoride using alumina.

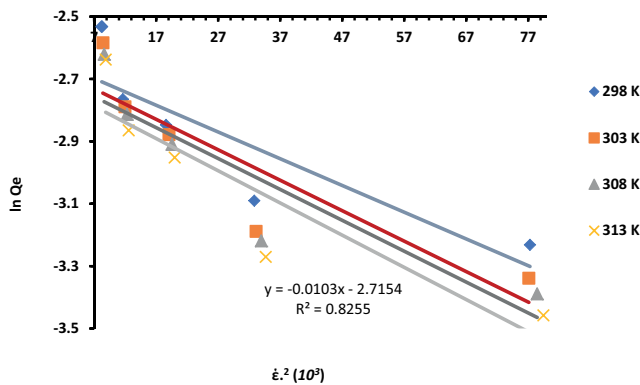


Fig. 4. Plots of D–R isotherm model for the removal of fluoride using alumina.

The D–R plots for adsorption of fluoride ion on alumina are presented in Fig. 6. Values of  $q_D$  and  $\beta_D$  were computed from the intercept and slopes of the respective plots and the mean free energy of sorption  $E$  was calculated by using the equation:

$$E = (2\beta_D)^{-1/2} \tag{7}$$

The mean free energy provides the nature of adsorption process. If  $E$  value equal 8 kJ/mol it suggests physisorption, if  $E$  value lies within 8–16 kJ/mol it suggests ion exchange process and  $E$  value greater 16 kJ/mol it suggests chemisorption [24].

The data regarding respective parameters of each of the isotherm model is presented in the Table 1. The Langmuir’s monolayer capacity ranged within 0.15–0.19 mg/g and were in ascending manner with temperature. Table 1 also shows the values of separation factor ( $R_L$ ) in the Langmuir isotherm lying between 0 and 1. The theory related to Langmuir model suggest that values of  $R_L$  within 0 and 1 indicate the feasibility of the adsorption process [25]. Similarly, the values of  $1/n$  which shows the surface inhomogeneity in the Freundlich model are generally lower than unity and approaching towards 1 with increasing

Table 1  
Values of parameters related to the two isotherms

Isotherms models	Parameters	Values			
		298 K	303 K	308 K	313 K
Langmuir	$K_L$	0.04	0.03	0.03	0.02
	$Q_{max}$	0.15	0.17	0.17	0.19
	$R_L$	0.21	0.26	0.28	0.32
	$R^2$	0.82	0.78	0.81	0.73
Freundlich	$n$	1.71	1.51	1.47	1.39
	$K_f$	0.01	0.01	0.01	0.01
	$1/n$	0.58	0.66	0.68	0.72
D–R	$R^2$	0.95	0.96	0.97	0.97
	$q_D$	0.07	0.07	0.07	0.07
	$\beta_D (10^{-3})$	8.60	9.80	9.90	10.30
	$E$ (kJ/mol)	0.008	0.007	0.007	0.007
	$R^2$	0.77	0.80	0.82	0.83

temperature (0.58–0.72 from 298–303 K). This indicates the loss of surface heterogeneity with little influence of chemisorption, that is, cooperative adsorption [26]. Mean free energy ( $E_s < 8$  kJ/mol) by D–R model reflects the weak Vander Waal interaction, that is, physical interaction between adsorbate–adsorbent system [27]. However, as per the values of co-efficient of determination ( $R^2$ ) it is evident that the adsorption data is more compatible with the Freundlich isotherm than with Langmuir and D–R isotherm models.

The defluoridation mechanism of alumina has been reported to be the exchange of  $F^-$  from aqueous media with the  $OH^-$  in the alumina adsorbent structure via the complex formation which has been confirmed by the MAS NMR spectroscopy [15].

### 3.1.6. Kinetic studies

To design a batch adsorption system kinetic studies are essential as they provide valuable information regarding the reaction pathways and the mechanism of adsorption process in addition to the rate at which a pollutant is

removed at the solid–solution interface [28]. To sever this purpose, the adsorption kinetic data has been applied on two kinetic models namely Lagergren’s pseudo-first-order and Ho’s pseudo-second-order models to illustrate the best fitting model. Additionally, intra particle diffusion model has also been utilized to see the solute transport from solution to the adsorbent.

Pseudo-first-order model assumes that adsorption of adsorbate ion on to the adsorbents surface is reversible. Therefore, this model is used to compare kinetics of system near equilibrium. The linear form of Lagergren’s pseudo-first-order can be presented in linear form as follows [29].

$$\ln(Q_e - Q_t) = Q_{lm} - kt \tag{8}$$

where  $Q_{lm}$  (mg/g) is Lagergren’s maximum sorption capacity and  $k$  ( $\text{min}^{-1}$ ) is rate constant and were obtained from the slope and intercept of  $\ln(Q_e - Q_t)$  against time  $t$ .

The Linear expression for the Ho’s pseudo-second-order model is [30]:

$$\frac{t}{Q_t} = \frac{1}{k_2 Q_e} + \frac{t}{Q_e} \tag{9}$$

where  $Q_e$ ,  $Q_t$  and  $t$ , have their usual meanings and  $k_2$  is the pseudo-second-order rate constant ( $\text{g/mg min}$ ) and was calculated from the slope and intercept of linear plot of  $t/Q_t$  against time  $t$ . Kinetics plot are presented in Figs. 5a and b and the parameters have been organized in Table 2 which shows that pseudo-second-order adsorption model is more fitting ( $R^2 = 0.999$ ) than pseudo-first-order model ( $R^2 = 0.493$ ). This is an indication that the rate of adsorption depends upon the concentration of fluoride as well as the number of active sites on the surface of the alumina adsorbent.

The intra-particle diffusion model can be used to describe the mode of solute transfer to the adsorbent during the

adsorption process. This model was developed by Weber and it considers that the adsorption capacity  $Q_t$  is related to  $\sqrt{t}$  linearly as given in Eq. (7). If the plot of  $Q_t$  vs.  $\sqrt{t}$  is a single straight line, then the adsorption is most probably controlled by intraparticle diffusion. However, if the same plot yields two straight lines then two or more steps influence the adsorption process [31].

$$Q_t = K_{id} t^{1/2} + C_{id} \tag{10}$$

where  $K_{id}$  ( $\text{mg/g min}^{1/2}$ ) and  $C_{id}$  are the intra-particle diffusion constant.

Sorption capacity at different time  $Q_t$  was plotted against  $\sqrt{t}$  and two straight lines were obtained as shown in Fig. 6 attributed to the boundary layer diffusion and intraparticle diffusion since the initial line doesn’t intersect the origin this indicates that surface phenomenon is complex, that is, both surface adsorption as well as intraparticle play a part in rate-limiting step [21].

### 3.1.7. Thermodynamic studies

The thermodynamic parameters like entropy  $\Delta S^\circ$ , enthalpy  $\Delta H^\circ$ , and Gibbs free energy  $\Delta G^\circ$  were calculated using the following equations:

$$\Delta G^\circ = -RT \ln(K_D) \tag{11}$$

$$\Delta G^\circ = \Delta H^\circ - T\Delta S^\circ \tag{12}$$

$$\ln(K_D) = \frac{\Delta S^\circ}{R} - \frac{\Delta H^\circ}{RT} \tag{13}$$

where  $T$  is the absolute temperature,  $R$  (J/mol K) is the gas constant,  $K_D$  is equilibrium constant of Van’t Hoff equation. The values of entropy  $\Delta S^\circ$  and enthalpy  $\Delta H^\circ$  were calculated

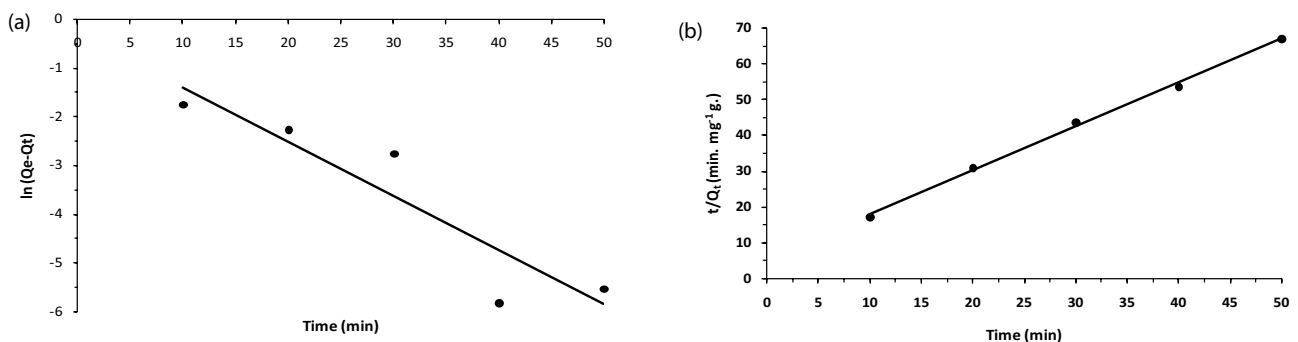


Fig. 5. Plot of (a) pseudo-first-order and (b) pseudo-second-order kinetics for the removal of fluoride using alumina.

Table 2  
Kinetics of adsorption and its parameters

Order of reaction	Slope	Intercept	Rate constant	Constants	$R^2$
Pseudo-first-order	-0.1111	-0.2815	$k$	$Q_{lm}$ 0.75	0.8483
Pseudo-second-order	1.2195	6.0168	$k_2$	$Q_e$ 0.82	0.9974

from the slope and intercept of the linear Van't Hoff plot of  $\ln(K_D)$  vs.  $1/T$  as shown in Fig. 7.

Table 3 represents the values of  $\Delta H^\circ$ ,  $\Delta S^\circ$ , and  $\Delta G^\circ$ . The values of  $\Delta G^\circ$  are negative and decreases with temperature indicates that adsorption is spontaneous and favorable at higher temperature [32]. Furthermore, free energy  $\Delta G^\circ$  values lies within  $-10$  kJ/mol suggests that process is physisorption. The positive values of  $\Delta H^\circ$  and  $\Delta S^\circ$  suggest the reflects endothermic nature and increase in randomness at the solid–solution interface during adsorption due to some surface changes [33]. Whereas,  $\Delta H^\circ$  values decreasing, and  $\Delta S^\circ$  are almost constant with increasing temperature.

### 3.2. Column studies

Dynamic mode studies were conducted using glass column of height 33 cm, internal diameter 3.4 cm provided with a frit of zero size. 5.0 g of alumina and initial fluoride concentration of 10 mg/L at ambient temperature and pH were introduced into the column. The average flow rate was set at 10 mL/min and concentration of influent and effluent was measured using ISE. Known amount of alumina was washed with deionized water to remove insoluble fine alumina dust particles. These dust particles may lead to the blocking of column frit. After washing, sample was oven dried at 105°C prior to use for the further study.

#### 3.2.1. Breakthrough curve studies

Breakthrough curve was studied to estimate the breakthrough sorption capacity (i.e., mg of F<sup>-</sup>/g of alumina) in

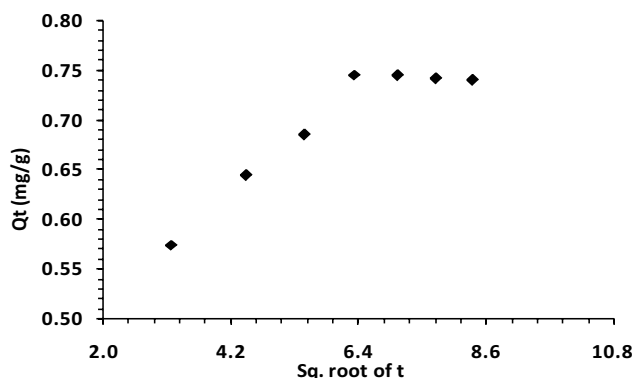


Fig. 6. Plot of intra particle diffusion model for the removal of fluoride using alumina.

which residual F<sup>-</sup> level in effluent was monitored until it reaches the WHO prescribed limit of F<sup>-</sup> in drinking water (i.e., 1.5 mg/L). Fig. 8 shows plot of F<sup>-</sup> in effluent as a function of volume of fluoride solution. It indicates that the fluoride concentration in the effluent is low for a range of volume but after the passage of solution volume of about 1.9 L, the concentration starts increasing until when a volume of 2.8 L is passed it becomes closer to the WHO limit of 1.5 mg/L. This point was called the breakthrough point where it corresponds to an adsorption capacity of 4.98 mg of F<sup>-</sup> per g of alumina.

#### 3.2.2. Exhaustion point studies

After breakthrough point, the column studies were extended to a complete saturation of the adsorbent. It was observed that for a complete cycle it consumed 7.1 L of 10.4 mg/L initial F<sup>-</sup> and which was called the exhaustion point wherein, F<sup>-</sup> level in influent and effluent were closer as shown in Fig. 9. The pattern of the curve represents the multilayer formation which is also confirmed by the compatibility of the data with the Freundlich model. The amount of F<sup>-</sup> absorbed per unit mass of alumina was 140 mg/g.

#### 3.2.3. Models for column studies

The column adsorption data was incorporated on Thomas, Yoon–Nelson, and Adam–Bohart models. Thomas model is based on Langmuir isotherm and the second-order kinetics models. [34]. It has been applied to predict the breakthrough curves and estimate adsorption capacity [35]. Ideally, the model is suitable in assessing

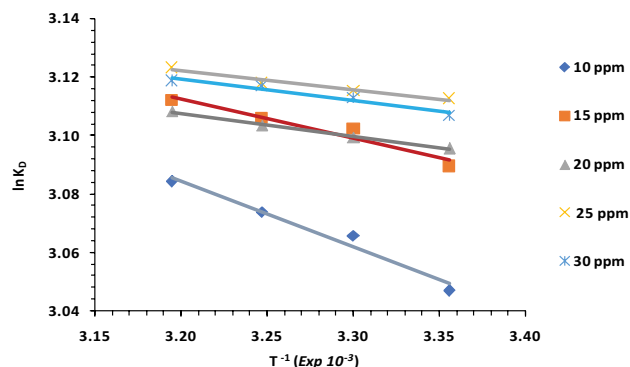


Fig. 7. Vant Hoff's plot for the removal of fluoride using alumina.

Table 3  
Thermodynamic parameters and their values

Concentration (ppm)	$\Delta H^\circ$ (kJ/mol)	$\Delta S^\circ$ (kJ/mol)	$\Delta G^\circ$ (kJ/mol)			
			298 K	303 K	308 K	313 K
10	1.87	0.0316	-7.56	-7.71	-7.87	-8.03
15	1.11	0.0294	-7.66	-7.81	-7.95	-8.10
20	0.66	0.0280	-7.67	-7.81	-7.95	-8.09
25	0.53	0.0277	-7.71	-7.85	-7.99	-8.13
30	0.62	0.0279	-7.70	-7.84	-7.98	-8.12

the adsorption systems where external/internal diffusion resistances are exceptionally small (favors intraparticle diffusion) [36]. The linear form of above model is [37]:

$$\ln \frac{C_i}{C_f} - 1 \frac{\dot{Q}}{Q} = \frac{K_{TH} Q_m}{Q} - K_{TH} C_i t \quad (14)$$

where  $C_i$ ,  $C_f$ , and  $t$  have their usual meanings  $m$  is mass (g),  $Q$  is flow rate (mL/min),  $K_{TH}$  (L/min mg) is Thomas kinetic coefficient and  $Q_m$  (mg/g) is breakthrough sorption capacity. Slope and intercept of linear plot of  $\ln(C_i/C_f - 1)$  against time  $t$  (min) were used to determine  $K_{TH}$  and  $Q_m$  as shown in Figs. 10a–c.

Adams–Bohart model is based on assumption that rate of adsorption depends upon surface reaction between residual vacant sites on the adsorbent and the concentration of the adsorbate [38]. This model is useful for the description of initial part of the breakthrough curve and mathematically Adam–Bohart Model expressed as [37]:

$$\ln \frac{C_f}{C_i} = K_{AB} C_i t - \frac{K_{AB} N_0 Z}{U_0} \quad (15)$$

where  $K_{AB}$  (L min/g) is Adam–Bohart constant,  $N_0$  is maximum uptake capacity per unit volume (mg/L),  $U_0$  linear

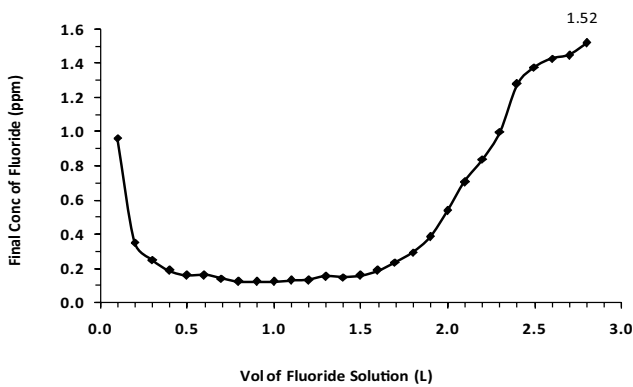


Fig. 8. Break through curve for the removal of fluoride.

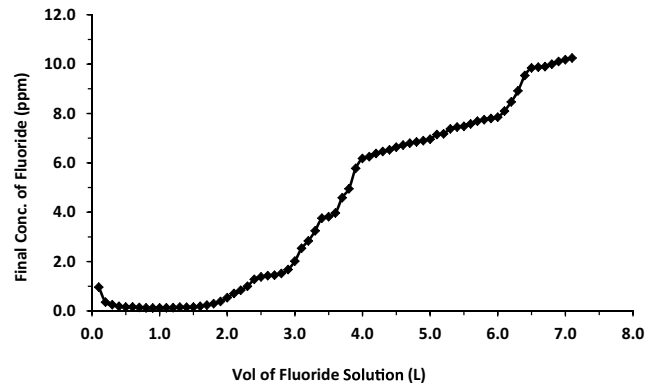


Fig. 9. Exhaustion curve of alumina for removal of fluoride.

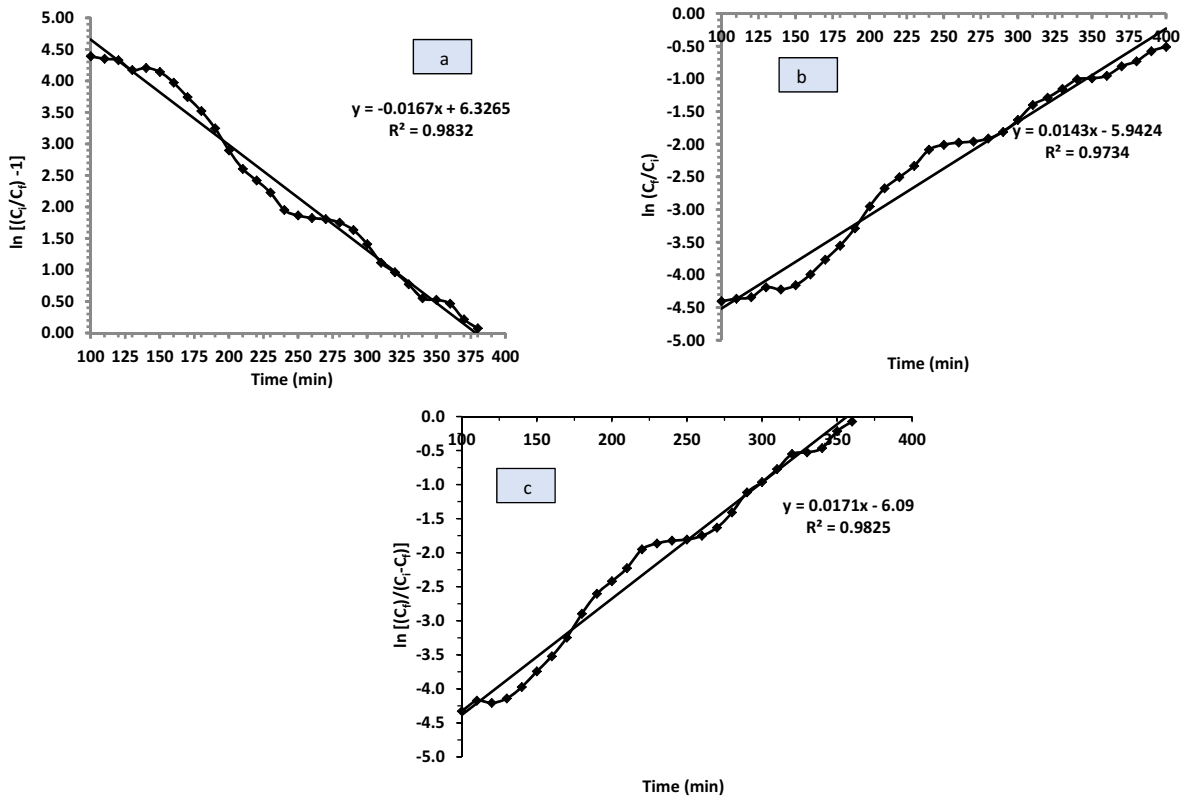


Fig. 10. (a) Thomas, (b) Adam–Bohart, and (c) Yoon–Nelson model for fluoride removal in alumina column.

velocity (cm/min),  $Z$  is the bed depth (cm). The values of  $K_{AB}$ ,  $N_0$  were obtained from the linear plot of  $\ln(C_f/C_i)$  against time  $t$  as shown in Figs. 10a–c.

Yoon–Nelson model assumes that the rate of decrease in the probability of adsorption is directly related to the probability of adsorbate adsorption and the probability of breakthrough on the adsorbent. The purpose of this model is to predict the time of column regeneration or replacement. The major advantage of using this model is that it is independent of detailed data regarding the type of adsorbent, characteristics of adsorbate, and physical properties of adsorbent bed. This model is expressed as [39]:

$$\ln \frac{C_f}{C_i - C_f} = K_{YN} t - K_{YN} \tau \quad (16)$$

where  $K_{YN}$  ( $\text{min}^{-1}$ ) is Yoon–Nelson rate constant,  $\tau$  (min) is the time required for 50% break through and their values were obtained from the slope and intercepts of the plots of  $\ln(C_f/C_i - C_f)$  against time  $t$  as shown in Figs. 10a–c.

Column models along with their parameters have been organized in Table 4 which describes dynamic mechanism of adsorption, the maximum adsorption capacity  $Q_m$  and the rate constant  $K_{TH}$  obtained via Thomas model were found to be 8.82 mg/g and 0.0012 L/min mg, respectively, at an initial concentration of 10 mg/L. Since the increase in concentration creates a concentration gradient between solid–liquid phase of adsorbate–adsorbent system therefore for a constant flow rate and column diameter values of  $Q_m$  were found to decrease and  $K_{TH}$  increased with rising the initial fluoride concentration [37].

The column adsorption data when fitted to the Adam–Bohart model retrieved the values of  $K_{AB}$  and  $N_0$  as 0.0007 L/mg min and 204.93 mg/L, respectively, and the values represented an undulant pattern with the initial concentration. Similarly, application of data on Yoon–Nelson model returned the values of  $K_{YN}$  and  $\tau$  as 0.0128  $\text{min}^{-1}$  and 426.83 min, respectively, furthermore,  $K_{YN}$  values were in ascending and  $\tau$  values were in descending relationship with the increasing initial concentration of fluoride. Lower concentration gradient causes a slower transport due to decreased diffusion coefficient or mass transfer coefficient. The decrease in breakthrough time with increasing inlet concentration is associated with quick saturation of the binding and ion exchange sites of adsorbent [40].

The three models generally produced high values of determination coefficient ( $R^2$ ) at each concentration levels but evidently, the data was found to be more compatible with Thomas and Yoon–Nelson model with the higher data fitting at high concentration of initial fluoride solution.

### 3.2.4. Desorption studies

Desorption efficiency of NaOH was optimized to regenerate the exhausted column. For this reason, NaOH solutions of different strengths (0.5%, 1%, 2%, 3%, and 4%) were passed through loaded column and promising results were obtained by 2% and 3% strength solutions, however, 1%, strength solution yielded more comprehensive

results. At higher strength (3%–4%) number of  $\text{OH}^-$  ions increases, therefore, electrostatic repulsion between  $\text{OH}^-$  and  $\text{F}^-$  decreases the desorption capacity of NaOH. That's why NaOH solution of 1% strength was considered as optimum for desorption studies. Desorption studies were extended using 1% NaOH solution on exhausted column and 455 mg of adsorbed fluoride was successfully desorbed, out of 495 mg of adsorbed fluoride with 92% desorption efficiency as shown in Table 5.

### 3.3. Pilot scale studies

Performance of pilot plant was scrutinized for the designing of real time defluoridation plant. For this purpose, pilot plant was designed containing a bed of 60 kg alumina on which numerous runs of large volume (avg. 860 L) of  $\text{F}^-$  (avg. 10.00 mg/L) were passed on daily basis. The defluoridated water samples were collected at initial, middle and near the end of each run to analyze residual  $\text{F}^-$  concentration. Mean values of residual fluoride were used to determine removal efficiency. Freshly prepared  $\text{F}^-$  solution was passed through pilot plant every day. Same procedure was repeated till the breakthrough point at 1.5 mg/L was achieved.

During the first cycle, 24 runs of each 860 L were found to be enough to achieve break through point with total volume of 20,640 L having average initial  $\text{F}^-$  concentration 9.67 mg/L. Break through sorption capacity was found to be 2.85 mg/g with 85.21% removal efficiency. Similarly, for second cycle, breakthrough point was achieved after passing 20 runs of each 860 L, with total volume of 17,200 L having average initial  $\text{F}^-$  concentration 10.60 mg/L. Break through sorption capacity was found to be 2.62 mg/g with 85.29% removal efficiency. The breakthrough capacity as well as breakthrough volume decreased further after the third cycle as shown in Table 6.

Table 4  
Column models parameters

Thomas model					
Conc. (mg/L)	Slope	Intercept	$K_{TH}$	$Q_m$	$R^2$
10	-0.0124	5.317	0.0012	8.82	0.9514
15	-0.0152	3.954	0.0015	5.35	0.9422
20	-0.0261	4.379	0.0025	3.45	0.9939
Adam–Bohart model					
Conc. (mg/L)	Slope	Intercept	$K_{AB}$	$N_0$	$R^2$
10	0.0071	-4.193	0.0007	204.93	0.8231
15	0.0082	-3.980	0.0005	247.29	0.8622
20	0.0101	-3.160	0.0005	209.84	0.8867
Yoon–Nelson model					
Conc. (mg/L)	Slope	Intercept	$K_{YN}$	$\tau$	$R^2$
10	0.0128	-5.463	0.0128	426.83	0.9452
15	0.0152	-5.318	0.0152	349.86	0.9422
20	0.0256	-5.303	0.0256	207.16	0.9947

Table 5  
Results of desorption study by 1% NaOH

Volume (mL)	Initial amount (mg)	Effluent conc. (mg/L)	Amount desorbed (mg)	% Desorption
200	495.0	1,280.0	256.0	51.7
400	239.0	512.0	128.0	53.6
700	111.0	129.0	32.3	29.1
1,000	78.8	48.0	14.4	18.3
1,200	64.4	32.1	6.4	10.0
1,400	57.9	23.0	4.6	7.9
1,600	53.3	22.3	4.5	8.4
1,800	48.9	22.4	4.5	9.2
2,000	44.4	21.0	4.2	9.5
Total	495.0		454.8	91.9

Table 6  
Results from pilot plant experiments

cycles	Breakthrough volume (L)	Breakthrough capacity (mg/g)
1	20,640	2.85
2	17,200	2.62
3	12,000	2.44

#### 4. Conclusion

Alumina was successfully applied for defluoridation studies. It was concluded that adsorption mechanism of fluoride on alumina was physisorption, that is, there exist some Van der Waal interactions between fluoride ions and alumina surface, and it follows Freundlich model. Furthermore, the process was endothermic and spontaneous (i.e., positive  $\Delta H^\circ$  and negative  $\Delta G^\circ$  values), dominating at higher temperature and follows the pseudo-second-order kinetics. In column studies, considering the fluoride limit set by WHO for drinking water breakthrough was set accordingly. Alumina offered 4.98 mg/g breakthrough sorption capacity. Optimized NaOH (1% W/V) used as regenerant, efficiently removing around 92% of the adsorbed fluoride from alumina which was saturated with 495 mg of fluoride. Above work was successfully protracted on pilot scale level which could provide around 20,000 L of water with safe fluoride levels in the first cycle. The breakthrough volume decreased to 17,000 and 12,000 L subsequently in the second and third cycles, respectively. These results have been extensive and extremely encouraging to design and engineer the real time defluoridation plant which will serve the under-privileged population of Thar desert in terms of their basic right of fluoride-safe drinking water.

#### References

- [1] WHO, Guidelines for Drinking-Water Quality, WHO Chronicle, World Health Organization, 2011, pp. 370–373.
- [2] M.-H. Yu, Chapter 10: Environmental Fluoride, In: Environmental Toxicology: Impacts of Environmental Toxicants on Living Systems, Lewis Publishers, Wahsington, DC, 2001, pp. 239.
- [3] T. Rafique, S. Naseem, D. Ozsvath, R. Hussain, M.I. Bhangar, T.H. Usmani, Geochemical controls of high fluoride groundwater in Umardkot Sub-District, Thar Desert, Pakistan, *Sci. Total Environ.*, 530 (2015) 271–278.
- [4] A. Banerjee, Groundwater fluoride contamination: a reappraisal, *Geosci. Front.*, 6 (2015) 277–284.
- [5] J. Nouri, A.H. Mahvi, A. Babaei, E. Ahmadpour, Regional pattern distribution of groundwater fluoride in the Shush aquifer of Khuzestan County, Iran, *Fluoride*, 39 (2006) 321–325.
- [6] T. Rafique, S. Naseem, M.I. Bhangar, T.H. Usmani, Fluoride ion contamination in the groundwater of Mithi sub-district, the Thar Desert, Pakistan, *J. Environ. Geol.*, 56 (2008) 317–326.
- [7] R. Tekle-Haimanot, Z. Melaku, H. Kloos, C. Reimann, W. Fantaye, L. Zerihun, K. Bjorvatn, The geographic distribution of fluoride in surface and groundwater in Ethiopia with an emphasis on the Rift Valley, *Sci. Total Environ.*, 367 (2006) 182–190.
- [8] K. Brindha, R. Rajesh, R. Murugan, L. Elango, Fluoride contamination in groundwater in parts of Nalgonda District, Andhra Pradesh, India, *Environ. Monit. Assess.*, 172 (2011) 481–492.
- [9] D.L. Ozsvath, Fluoride and environmental health: a review, *Rev. Environ. Sci. Biotechnol.*, 8 (2009) 59–79.
- [10] S. Grobler, A. Louw, V.W. Kotze, Dental fluorosis and caries experience in relation to three different drinking water fluoride levels in South Africa, *Int. J. Paediatr. Dent.*, 11 (2001) 372–379.
- [11] I. Ahmed, T. Rafique, S.K. Hasan, N. Khan, M.H. Khan, T.H. Usmanib, Correlation of fluoride in drinking water with urine, blood plasma, and serum fluoride levels of people consuming high and low fluoride drinking water in Pakistan, *Fluoride*, 45 (2012) 384–388.
- [12] M. Mohapatra, S. Anand, B.K. Mishra, D.E. Giles, P. Singh, Review of fluoride removal from drinking water, *J. Environ. Manage.*, 91 (2009) 67–77.
- [13] A. Bhatnagar, E. Kumar, M. Sillanpää, Fluoride removal from water by adsorption—a review, *Chem. Eng. J.*, 171 (2011) 811–840.
- [14] H.M. Maurice S. Onyango, Fluoride Removal from Water Using Adsorption Technique, A. Tressaud, Ed., Fluorine and the Environment: Agrochemicals, Archaeology, Green Chemistry and Water, Elsevier Science, Amsterdam, 2006, pp. 1–48.
- [15] E. Kumar, A. Bhatnagar, U. Kumar, M. Sillanpää, Defluoridation from aqueous solutions by nano-alumina: characterization and sorption studies, *J. Hazard. Mater.*, 186 (2011) 1042–1049.
- [16] W.-X. Gong, J.-H. Qu, R.-P. Liu, H.-C. Lan, Adsorption of fluoride onto different types of aluminas, *Chem. Eng. J.*, 189–190 (2012) 126–133.

- [17] P. Chinnakoti, A.L. Chunduri, R.K. Vankayala, S. Patnaik, V. Kamiseti, Enhanced fluoride adsorption by nano crystalline  $\gamma$ -alumina: adsorption kinetics, isotherm modeling and thermodynamic studies, *Appl. Water Sci.*, 7 (2017) 2413–2423.
- [18] J.-Y. Lin, Y.-L. Chen, X.-Y. Hong, C. Huang, C. Huang, The role of fluoroaluminate complexes on the adsorption of fluoride onto hydrous alumina in aqueous solutions, *J. Colloid Interface Sci.*, 561 (2020) 275–286.
- [19] H. Zarei, S. Nasser, R.N. Noudehi, S. Pourfadakari, F. Shemirani, A.H. Mahvi, Evaluation of removal efficiency of fluoride from aqueous solutions using synthesis of nano-scale alumina on multi walled carbon nanotube (MWCNTs): equilibrium and kinetic studies, *Desal. Water Treat.*, 65 (2017) 359–366.
- [20] S. Ghorai, K. Pant, Investigations on the column performance of fluoride adsorption by activated alumina in a fixed-bed, *Chem. Eng. J.*, 98 (2004) 165–173.
- [21] S. Ghorai, K. Pant, Equilibrium, kinetics and breakthrough studies for adsorption of fluoride on activated alumina, *Desal. Water Treat.*, 42 (2005) 265–271.
- [22] G.J. Millar, S.J. Couperthwaite, L.A. Dawes, S. Thompson, J. Spencer, Activated alumina for the removal of fluoride ions from high alkalinity groundwater: new insights from equilibrium and column studies with multicomponent solutions, *Desal. Water Treat.*, 187 (2017) 14–24.
- [23] S.S. Tripathy, J.-L. Bersillon, K. Gopal, Removal of fluoride from drinking water by adsorption onto alum-impregnated activated alumina, *Desal. Water Treat.*, 50 (2006) 310–317.
- [24] A. Daifullah, S. Yakout, S. Elreefy, Adsorption of fluoride in aqueous solutions using  $\text{KMnO}_4$ -modified activated carbon derived from steam pyrolysis of rice straw, *J. Hazard. Mater.*, 147 (2007) 633–643.
- [25] X. Wang, C. Jiang, B. Hou, Y. Wang, C. Hao, J. Wu, Carbon composite lignin-based adsorbents for the adsorption of dyes, *Chemosphere*, 206 (2018) 587–596.
- [26] K.Y. Foo, B.H. Hameed, Insights into the modeling of adsorption isotherm systems, *Chem. Eng. J.*, 156 (2010) 2–10.
- [27] J. Shi, Z. Zhao, Z. Liang, T. Sun, Adsorption characteristics of Pb(II) from aqueous solutions onto a natural biosorbent, fallen arborvitae leaves, *Water Sci. Technol.*, 73 (2016) 2422–2429.
- [28] Y.-S. Ho, G. McKay, Pseudo-second order model for sorption processes, *Process Biochem.*, 34 (1999) 451–465.
- [29] H. Qiu, L. Lv, B.-c. Pan, Q.-j. Zhang, W.-m. Zhang, Q.-x. Zhang, Critical review in adsorption kinetic models, *J. Zhejiang Univ. Sci. A*, 10 (2009) 716–724.
- [30] Y.-S. Ho, G. McKay, Kinetic models for the sorption of dye from aqueous solution by wood, *Process Saf. Environ. Prot.*, 76 (1998) 183–191.
- [31] C. Valderrama, X. Gamisans, X. De las Heras, A. Farran, J. Cortina, Sorption kinetics of polycyclic aromatic hydrocarbons removal using granular activated carbon: intraparticle diffusion coefficients, *J. Hazard. Mater.*, 157 (2008) 386–396.
- [32] N.Y. Mezenner, A. Bensmaili, Kinetics and thermodynamic study of phosphate adsorption on iron hydroxide-eggshell waste, *Chem. Eng. J.*, 147 (2009) 87–96.
- [33] Z. Wu, H. Zhong, X. Yuan, H. Wang, L. Wang, X. Chen, G. Zeng, Y. Wu, Adsorptive removal of methylene blue by rhamnolipid-functionalized graphene oxide from wastewater, *Water Res.*, 67 (2014) 330–344.
- [34] K.H. Chu, Fixed bed sorption: Setting the record straight on the Bohart–Adams and Thomas models, *J. Hazard. Mater.*, 177 (2010) 1006–1012.
- [35] K. Vijayaraghavan, Y.-S. Yun, Bacterial biosorbents and biosorption, *Biotechnol. Adv.*, 26 (2008) 266–291.
- [36] R. Han, Y. Wang, X. Zhao, Y. Wang, F. Xie, J. Cheng, M. Tang, Adsorption of methylene blue by phoenix tree leaf powder in a fixed-bed column: experiments and prediction of breakthrough curves, *Desalination*, 245 (2009) 284–297.
- [37] A. Ahmad, B. Hameed, Fixed-bed adsorption of reactive azo dye onto granular activated carbon prepared from waste, *J. Hazard. Mater.*, 175 (2010) 298–303.
- [38] A. Jusoh, Y. Tam, A. Liew, M. Megat, K. Saed, Adsorption of remazol dye onto granular activated carbon in fixed bed: a case study of Red 3BS, *Int. J. Eng. Technol.*, 1 (2004) 58–63.
- [39] N. Yahaya, I. Abustan, M. Latiff, O.S. Bello, M.A. Ahmad, Fixed-bed column study for Cu(II) removal from aqueous solutions using rice husk based activated carbon, *Int. J. Eng. Technol. Innovation*, 11 (2011) 248–252.
- [40] Z. Aksu, F. Gönen, Z. Demircan, Biosorption of chromium(VI) ions by Mowital®B30H resin immobilized activated sludge in a packed bed: comparison with granular activated carbon, *Process Biochem.*, 38 (2002) 175–186.